*36th EPS Conference on Plasma Phys. Sofia, June 29 - July 3, 2009 ECA Vol.**33E**, P-2.146 (2009)*

Determination of Ni impurity density on JET by VUV emission spectroscopy

A. Czarnecka[1], J. Rzadkiewicz[1], K-D. Zastrow[2], I. H. Coffey[3], K. D. Lawson[2], M. G. O'Mullane[4] and JET-EFDA contributors*

JET-EFDA, Culham Science Centre, Abingdon, OX14 3DB, UK

[1]Institute of Plasma Physics and Laser Microfusion, EURATOM Association, Poland

[2]Euratom/UKAEA Fusion Association, Culham Science Centre, Abingdon, OX14 3DB, UK

[3]Astrophysics Research Centre, School of Mathematics and Physics, Queen's University, Belfast, BT7 1NN, Northern Ireland, UK

[4]Department of Physics, University of Strathclyde, Glasgow G4 0NG, UK

* See the Appendix of F. Romanelli et al., Fusion Energy Conference 2008 (Proc. 22nd Int. Conf. Geneva, 2008) IAEA, (2008)

Introduction

Studies of the impurity behaviour in large tokamak plasmas during additional heating is of fundamental interest because of the resulting increase in radiated power and ion dilution. In particular, mid- and high-Z impurities can contribute to the average Z_{eff} during high power radio frequency (RF) pulses. Furthermore, the VUV radiation emitted by the metallic impurities at the plasma edge affect the plasma density limit and the quality of the RF-induced H-modes. The impurity release from the screens of the RF antenna may significantly limit the heating effectiveness [1].

Since the metallic impurity radiation increases with the RF power and pulse duration, it is specially relevant to the assessment of the ITER-like antenna (ILA) in JET, where powers of up to 7.2MW are expected. This is facilitated by the provision of metallic impurity densities for large numbers of discharges and, to this end, a method for determining the densities in steady-state plasmas using passive spectroscopy is presented. In the first instance, this method has been applied to Ni, the commonest metallic impurity observed in JET.

Experimental arrangement

The determination of Ni impurity density relies on the absolutely calibrated measurements of the intensity radiation emitted by Li-like Ni [2]. Measurements were performed by means of survey SPRED spectrometer (KT2 JET diagnostic [2-4]). The spectrometer typically registers VUV spectra in the wavelength range of 100–1100 Å with an approximate spectral resolution of 5Å. The detector consists of a microchannel plate coated with CuI and a phosphor coupled by a fibre optic bundle to a 2048 photodiode array. Its line of sight is along the vessel midplane via a spherical mirror (Au coating) with an angle of incidence of 75° that reduces the sensitivity of about 50%.

In the wavelength range scanned by the KT2 diagnostic one can observe six main lines originating from the Ni impurity, four being the Li-like and Na-like doublets

($2p^6 3s\ ^2S_{1/2} - 2p^6 3p\ ^2P_{1/2,3/2}$ and $1s^2 2s\ ^2S_{1/2} - 1s^2 2p\ ^2P_{1/2,3/2}$). At low wavelengths, the line that corresponds to the $1s^2 2s2p\ ^1P_1 - 1s^2 2s^2\ ^1S_0$ transition in Be-like Ni is seen; however, in this range the sensitivity of the SPRED spectrometer falls off sharply, leading to a less certain calibration. The calibration for the Li-like and Na-like doublets is most accurate, this being crucial for determining the absolute level of an impurity. Since, the aim of the analysis was to determine the Ni impurity density in core plasmas, we have used the most intense Li-like line at 165Å which is emitted from this region.

Method to determine the Ni impurity density

In contrast to the emission from the very centre of the plasma, for which coronal equilibrium can be assumed, the VUV lines are emitted from a range of plasma radii, at which transport must be considered, a factor that seriously complicates the routine precision of impurity data. The method used for determining of the Ni impurity density is based on the combination of absolutely calibrated VUV transition intensity measurements with Universal Transport Code (UTC) simulations [5]. In the analysis the line integrated measurements of the 165 Å transition of Li-like Ni have been used from test discharges characterised by widely varied electron temperature and density profiles (see Figure 1). The electron temperature and density profiles were taken from the LIDAR Thomson scattering [6] and electron cyclotron emission diagnostics [7], while the atomic data (ionisation, recombination and line emission coefficients) have been provided by the ADAS database [8]. In order to reproduce (by means of the UTC code) measured VUV line intensities, given the plasma profiles, atomic characteristics, the position of the flux surfaces (EFIT equilibrium) and diagnostic geometry have been provided. The particle influx from the plasma edge was a free parameter.

In simulations a wide class of transport coefficients (D, v), presented in Figure 2, has been considered in the region where the plasma emits the radiation originating from the Li-like Ni. The choice of the D and v profile sets have also been inspired by extended previous studies of the Z-dependence impurity transport [9]. Unlike other UTC inputs, transport coefficients where treated as unknown discharge parameters. Since only steady-state plasmas were investigated, the diffusion and convection velocity have been kept constant in time. For a given set of D(r) and v(r), the simulated line intensity was matched to that measured in the experiment. It is found that, in all simulations, the emissivity of the radiation originating from the Li-like Nickel integrated along the diagnostic line of sight peaks in the mid-radius region r/a ~ 0.5-0.6, where local electron temperatures range from 2 to 4.5 keV. Therefore the simulated Ni density (see Figure 3) at this radius varies only by 10-20%, with larger variations elsewhere. It has been observed that the largest statistical errors tended to occur for sets with low diffusion coefficients. An approximately linear dependence on the local electron temperature of the ratio between the derived Ni densities and the line intensity with an error of about 20 % has been obtained for r/a ~ 0.5 - 0.6. Results are shown in Figure 4. Each point on this figure corresponds to one plasma discharge

characterised by different plasma parameters. Error bars reflect variation of transport coefficients.

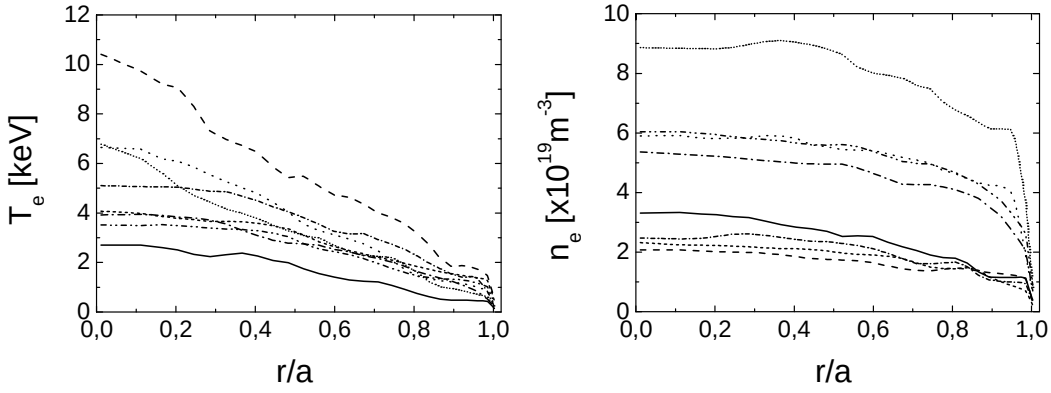

Figure 1. *Electron density and temperature profiles obtained from the LIDAR Thomson scattering and electron cyclotron emission diagnostics used in the UTC simulations to test different JET discharges. One T_e and one n_e profile has been used for each point in Figure 4.*

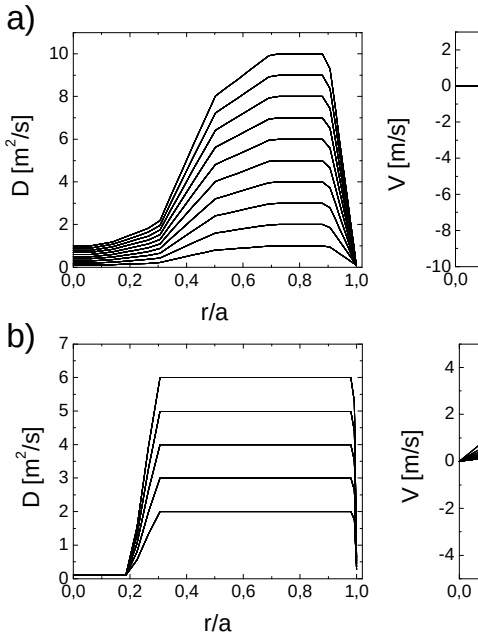

Figure 2a), b) *Sets of the diffusion D(r) and convection v(r) transport coefficients used in simulations as an unknown discharge parameter in the region where the Li-like emissions is coming from.*

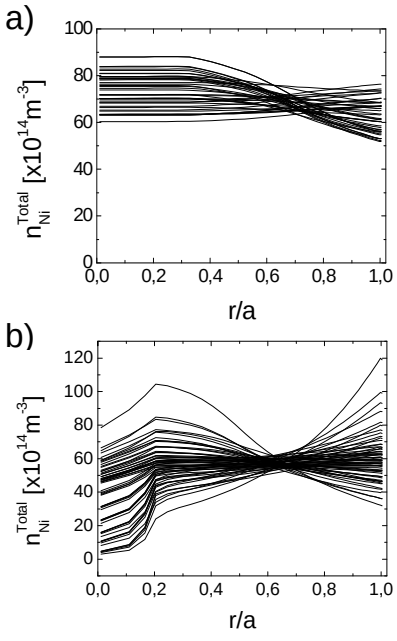

Figure 3. *Total Ni density profiles obtained by means of the UTC simulations for a wide class of transport coefficients a) presented in fig.2a, b) presented in fig.2b.*

The above linear fit is exploited to derive local Ni densities for all JET discharges during the divertor phase and the derived impurity density has been used to study Ni impurity trends with applied heating power for the different JET heating systems (see Figure 5b). Correlations between derived Ni density and applied heating power from the new ITER-like antenna (up to 4.76 MW coupled in L-mode) and the A2 antenna for different plasma scenarios are presented in Figure 5a.

A database of such correlations shows that the ILA for the same total power, but at a much higher power density up to 6.2 MW/m^2 produces the same amount of impurities as the A2s that have a much bigger surface and never reached in L-mode power density above 1.8 MW/m^2 [10].

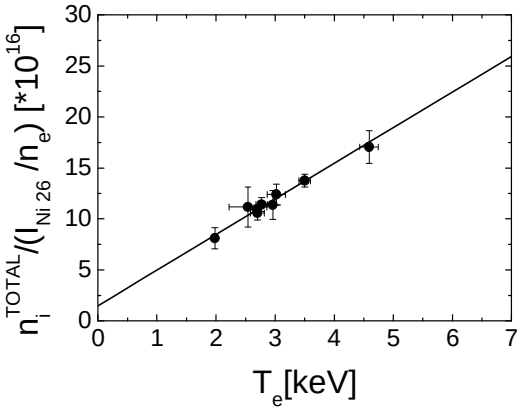

Figure 4*. Ratio of the simulated Ni impurity density to the experimental intensity of the $1s^22p\ ^2P_{3/2} - 1s^22s\ ^2S_{1/2}$ transition in Li-like Ni (normalized to the electron density) for mid-radius region as a function of the electron temperature.*

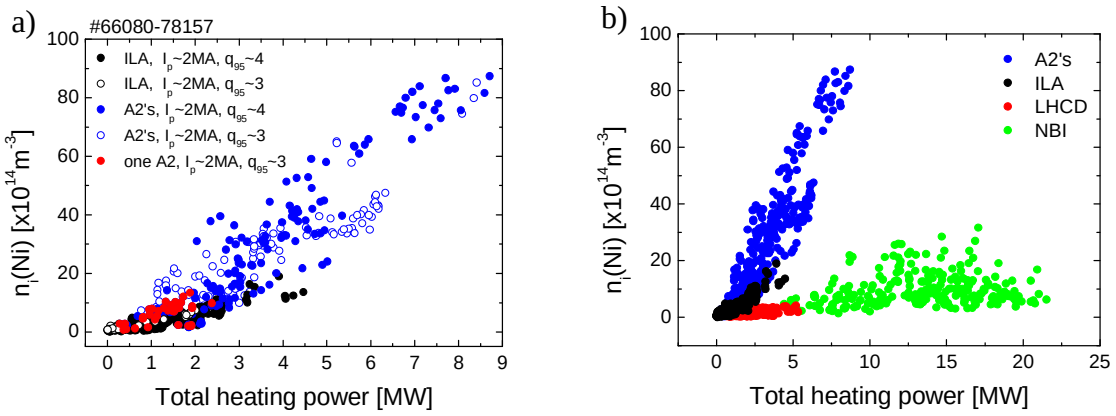

Figure 5*. Correlation between the derived Ni densities (r~0.5-0.6) and applied heating power for a) the RF heating systems. b) the different JET heating systems.*

Acknowledgments

This work, supported by the European Communities under the contract of Association between EURATOM/Polish Association, was carried out within the framework of the European Fusion Development Agreement. The views and opinions expressed herein do not necessarily reflect those of the European Commission.

References

[1] M. Bures et al., Plasma Phys. Control. Fusion, vol. 33, No.8, 937 (1991)
[2] K. D. Lawson et al., JINST 4 P04013 (2009)
[3] I. H. Coffey, Rev. Sci. Instrum., 75 (10), 3737 (2004)
[4] R. J. Fonck et al., Appl.Opt., 21, 2115 (1982)
[5] A. D. Whiteford et al., 31st EPS Conference, ECA vol. 28G P–1.159, (2004)
[6] C. Gowers et al., Rev. Sci. Instrum., 66, 471 (1995)
[7] E. De La Luna et al., Rev. Sci. Instrum., 75, 3831 (2004)
[8] H. P. Summers 2000, The ADAS User Manual version 2.7, http://www.adas.ac.uk
[9] C. Giroud et al., 31st EPS Conference, ECA vol. 28G P–5.159, (2004)
[10] M.-L. Mayoral et al., this conference